CrystEngComm

Accepted Manuscript

ROYAL SOCIETY OF CHEMISTRY

www.rsc.org/crystengcomm

Journal Name RSCPublishing

ARTICLE

Synthesis and Luminescence properties in H_2 annealing Mn-doped $Y_3Al_5O_{12}:Ce^{3+}$ single crystal for W-LEDs

Cite this: DOI: 10.1039/x0xx00000x

Received ooth January 2012,
Accepted ooth January 2012

DOI: 10.1039/x0xx00000x

www.rsc.org/

Guorui Gu,[a] Weidong Xiang,*[a] Cheng Yang,[a] Xiaojuan Liang,[a]

Czochralski grown Mn-doped $Y_3Al_5O_{12}:Ce^{3+}$ single crystal was thermally annealed in H_2 atmosphere at different temperature for 6 h and the corresponding absorption spectra, emission spectra, quantum yield (QY) and color-electric performance of Ce,Mn:YAG single crystal wafers were investigated before and after annealing, respectively. Moreover, electron paramagnetic resonance (EPR) of doped Mn ions and possible energy transfer process from Ce^{3+} to Mn^{2+} ion were discussed in detail. The corresponding results demonstrated that the H_2 annealing process partly generated the intensity of luminescence spectra and improved the value of quantum yield and luminous efficacy (LE). The H_2 annealing at 1550 □ is the most optimal annealing condition, after annealing, a maximum luminous efficacy reaching 119.93 lm/W, a color rendering index of 73.6 at a correlated color temperature of 5674 K is obtained, which demonstrates that Ce,Mn:YAG single crystal is expected to be an optimal candidate for white LED.

Introduction

Currently, white light-emitting diodes (W-LEDs), the next generation of solid state lighting, have attracted significant attention due to their excellent properties, such as high luminous efficacy, long lifetime, environment friendless, low energy consumption and magnificent applications for displays and lighting.[1-4] The leading commercial available white LED is manufactured by coating a blue emitting InGaN die with a cerium activated yttrium aluminum garnet (Ce^{3+}:$Y_3Al_5O_{12}$,Ce:YAG) phosphor packed onto the chip surface using epoxy resin or silicone.[5-8] However, for advanced high power white LED, this combination cannot provide long-term reliability owing to photo-degradation of the organic epoxy resin under condition of high irradiation and high temperatures, this easily brings some issues, such as chromatic aberration, luminous efficacy degradation, lifetime reduction and so on.[9] In order to conquer these problems, alternative phosphor conversion materials, which do not require the presence of epoxy resin, are suggested: (1) poly-crystalline Ce:YAG transparent ceramics.[10,11] (2) low melt-point glass mixture with Ce:YAG phosphor plates.[12] A reported maximum LE reaching 93 lm/W at a low correlated color temperature (CCT) of 4600 K was obtained in a thin transparent Ce:YAG ceramic-based WLED.[13,14] However, transparent ceramics require sophisticated

[a]College of Chemistry and Materials Engineering, Wenzhou University,Wenzhou, China.

*Corresponding author.Tel:+86 577 86596013; fax: +86 577 86689644.E-mail address: xiangweidong001@126.com.

and complex synthesis technology for obtaining optically transparent plates, the high fabrication cost is an unavoidable challenge for mass industrialization production of the transparent Ce:YAG ceramics, moreover, the quantum yield (QY) and luminous extraction of ceramic plates are lower than those of the commercial powder phosphors, owing to wave-guide loss and backward emission loss. For the low melt-point mixed with Ce:YAG phosphor plates, the concentration of Ce:YAG dispersed in glass matrix has an important influence on its stability, which raises a big limitation to this material, although adjusting the phosphor to glass ratio can produce comparable performance to the phosphor and resin mix, however, the glass will become very fragile. Lowered the percentage of phosphor particles can increase stability of the glass but at the same time, the ability to provide enough phosphorescence will be lost. All of these restrict its application and development in the field of white LED.

As all we know, the white LED based on YAG:Ce^{3+} phosphor exhibits a poor color rendering index and a high correlated color temperature because of lacking a red component.[15] Transition metal Mn^{2+} can provide a broad emission band in the visible (VIS) range corresponding to d-d transition, and its emission varies from green to red depending on the crystal field.[16] Since the absorption efficiency of d-d transition is low due to the spin- and parity-forbidden electricdipole transition, sensitizing ions (Eu^{2+}, Ce^{3+}, etc.) are often utilized to enhance the emission of Mn^{2+}. The energy transfer mechanism from a sensitizer to an activator has been investigated in many inorganic hosts, such as fluorides, silicates, phosphates, and borates.For example, Caldino et al.[17] reported that the $Ce^{3+}\rightarrow Mn^{2+}$ energy transfer and mechanism involved with CaF_2:Ce^{3+}, Mn^{2+} phosphor, the $Ce^{3+}\rightarrow Mn^{2+}$ energy transfer process to form small $Ce^{3+}\rightarrow Mn^{2+}$ complexes, and the $Ce^{3+}\rightarrow Mn^{2+}$ energy transfer was rationalized by assuming that a short-range interaction mechanism such as electric dipole-quadrupole interaction occurs in the $Ce^{3+}\rightarrow Mn^{2+}$ clusters. However, to the best of our knowledge, up to now, there is less report about Ce^{3+}/Mn^{2+} doped YAG single crystal and detail photoluminescence (PL) properties of the sensitization effect of Ce^{3+} to Mn^{2+} ions in YAG single crystal. Yu. Zorenko et al.[18] once reported the luminescent properties of Mn-doped $Y_3Al_5O_{12}$ single crystalline films, under excitation at 267 nm, the PL spectra of both SCF samples present the dominant luminescence of Mn^{3+} ions in the main band peaked at 608 nm and other low-intensive band peaked approximately at 760 nm, both related to the $^5T_2\rightarrow{}^5E$ transitions. V. Singh et al.[19] reported that the green emission at peak at 519 nm in Mn^{2+} activated $Y_3Al_5O_{12}$ is assigned to ^4T1_g (G) $\rightarrow{}^6A1_g$ (S) transition of Mn^{2+} ions.

In this paper, we suggest an innovative candidate, Czochralski (CZ) grown Ce,Mn:YAG single crystal as a yellow phosphor substitute to replace the traditional resin/silicone-based phosphor converter for WLED in current package. We attempt to dope manganese ion into YAG single crystal and expect to obtain the emission of Mn^{2+} in orange-red region via energy transfer (ET) between Ce^{3+} and Mn^{2+}, which will significantly improve the performance index of the white LED devices. Furthermore, the reasonable annealing process can decrease the concentration of oxygen vacancy derived from the crystal growth to partly improve the luminous efficacy of Ce,Mn:YAG single crystal wafers, which has been documented by the authors.[20] Therefore, we annealed Czochralski grown Ce,Mn:YAG single crystal in H_2 atmosphere at different temperature for 6 h and the corresponding absorption spectra, emission spectra, quantum yield (QY) and color-electric performance of Ce,Mn:YAG single crystal wafer were investigated before and after annealing, respectively. Especially, the EPR of doped Mn ions and possible energy transfer process from Ce^{3+} to Mn ions were also discussed in detail. Finally, a maximum

luminous efficacy reaching 119.93 lm/W, a color rendering index of 73.6 at a correlated color temperature of 5674 K is obtained at 1550□, which demonstrate that Ce,Mn:YAG single crystal is expected to be an optimal candidate for white LED.

Results and discussion

The photograph of the as-grown Ce,Mn:YAG single crystal is shown in Fig.1. Crystal is approximately 15 mm in diameter and 80 mm in length. It is transparent and bright red coloration.

Fig.1 As-grown Ce,Mn:YAG single crystal grown by Czochralski

XRD analysis

Shown in Figure.2 is the comparison of powder XRD patterns of Ce:YAG , Mn:YAG and Ce,Mn:YAG single crystal. All XRD patterns were found to agree well with JCPDS Card (No. 033-0040) and no peak was assigned to other crystalline phases, indicating that the doped Ce and Mn ions did not generate any impurity or induce significant changes in the host structure. Doped yttrium aluminum garnets (YAGs) are widely used materials for solid-state lasers. YAG belong to the cubic crystal system with distorted garnet structure, lattice parameters a = b = c = 12.009 Å, Y^{3+} ion (radius r = 1.019 Å) is coordinated with eight oxygen ions, some Al^{3+} (r = 0.535 Å) are six-fold coordinated and others are four-fold coordinated, respectively. In the crystallization process of single crystal , according to the ionic electronegativity scale[21,22], the eight coordinated Ce^{3+} ions (r = 1.143 Å) and Mn^{2+} (r = 0.96 Å) are easy to replace the Y^{3+} ions and be doped into the crystalline phase due to the close radius, electronegativity and valence with Y^{3+}, whereas six coordinated Mn^{2+} ions (r = 0.67 Å), Mn^{3+} ion (r = 0.58 Å) and Mn^{4+} ions (r = 0. 053 Å) tend to replace the lattice of Al^{3+} ions. The calculated cell parameters of Ce,Mn: YAG are a = b = c = 11.994 Å according to XRD data and decrease by 0.015 Å compared with the cell parameters of pure YAG, which can be ascribe to the smaller radius of doped Mn ions than Y^{3+}.

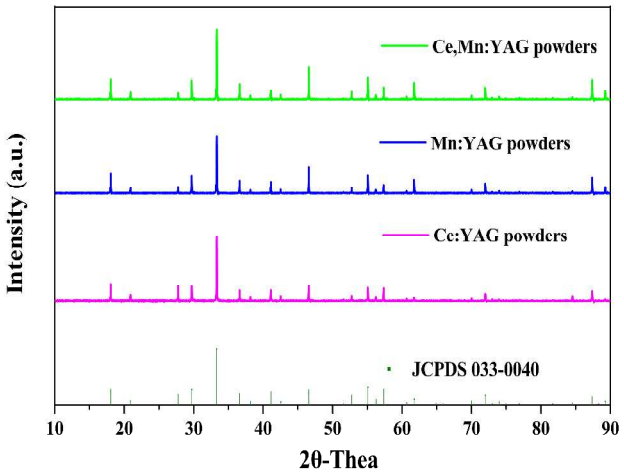

Fig.2 Comparison of powder XRD patterns of Ce:YAG , Mn:YAG and Ce,Mn:YAG single crystal

Electron Paramagnetic Resonance (EPR) of Mn ion

Manganese ion is a well-known activator used in YAG mainly for producing tunable solid-state laser media, holographic recording and optical data storage as well as thermo-luminescent detectors.[23] A peculiarity of doping by manganese is creation of different charge states of Mn ions (2+, 3+ and 4+) depending on the condition of crystallization, content of growth atmosphere and post-growth treatment, as well as the charge state of co-dopants.[24] The different charges of the Mn ions have different luminescence properties.[25] In this work, we use EPR spectroscopy for the accurate determination of different oxidation states of manganese in Ce,Mn:YAG single crystal. The EPR spectra of pure YAG and Ce: YAG crystal powder samples are also provided as comparison.

As all we know, the outer electrons of Ce^{2+} and Ce^{4+} are paired electrons, which will appear no signal in the EPR detection, while the Ce^{3+} ion has a single electron orbit, which can generate a resonance spectrum in the magnetic. However, as with all the lanthanides, the crystal field received by Ce^{3+} is weak field due to the shielding effects suffered from the outer electrons , which can be ascribed to the under-filled $4f^n$ shell electron of Ce^{3+}. Fig.3 depicts the EPR spectra of YAG and Ce: YAG crystal powder samples at room temperature.

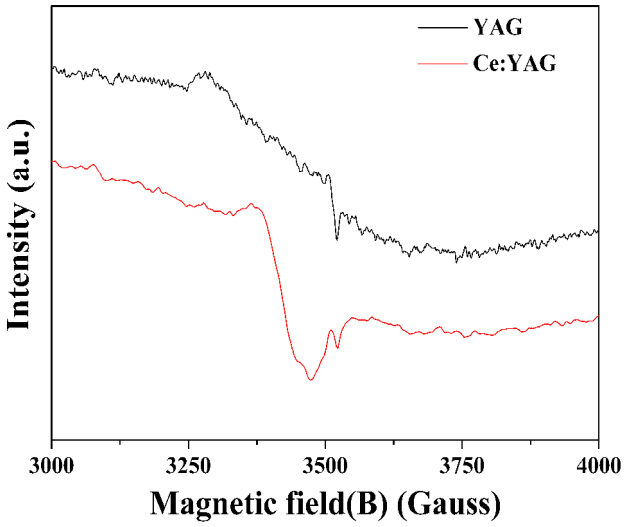

Fig.3 The EPR spectra YAG and Ce:YAG single crystals

Seen from the graph, the shape and trend of these two EPR spectra are roughly same, but the spectra line intensity of Ce: YAG samples at the magnetic field strength of 3482 G obviously increased, the characteristic peak of Ce^{3+} should appear at a magnetic field strength of 3550 G,[26] however, it does not appear. The possible reason is that the lowest energy level of the rare earths containing an odd number of electrons must be a Kramer double degenerate state after taking place an energy level splitting, and the EPR spectra usually must be observed at the temperature below 20 K due to the larger spin-orbit coupling interaction of Ce^{3+}. However, the EPR spectra of YAG and Ce:YAG single crystal in this paper are detected at room temperature, therefore the characteristic peak of Ce^{3+} does not appear. As for the enhanced spectrum line at the magnetic field strength of 3482 G, the possible reason is that the "color center" is formed in YAG due to the doping of Ce^{3+} ions, and as mentioned in the previous references,[27] YAG crystal doped with metal ions will appear the so-called "color center"at the magnetic field intensity of 3484 G and the spectral line intensity of "color center" will enhance with the increasing doping concentration of metal ion. The behaviour of the lowest energy levels of S state ions and particularly the ion Mn^{2+} has been studied in a number of crystals with different local symmetries.[28,29] EPR spectra of Mn^{3+} complexes in oxide crystals have been poorly investigated than those of $3d^4$ non-Kramers iron (Fe^{4+} ions). These ions exhibit large zero field splittings due to the influence of the Jahn-Teller effect on the ^{5}Eg ground state in octahedral symmetry.[29]

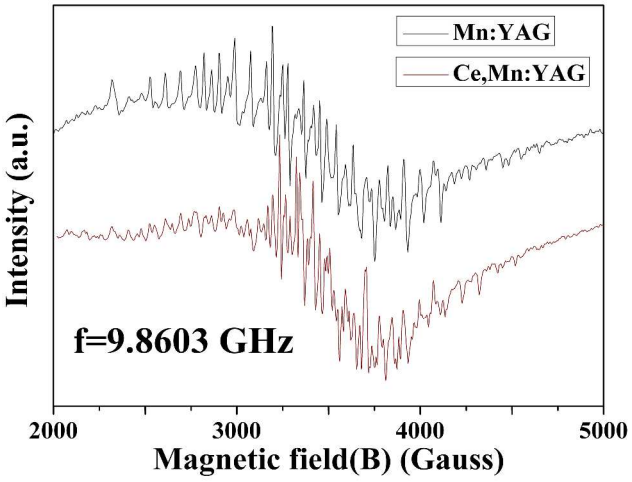

Fig.4 The EPR spectra of Mn:YAG and Ce,Mn:YAG crystals

Compared to the spectrum of YAG crystal in Fig.3, Mn: YAG and Ce, Mn:YAG single crystal samples both show the hyperfine structure of manganese with six lines which have the same resonance linewidths (6 sharp lines tagged with **a** from 3190 G to 3620 G are shown in the Fig.5) and the multiplet structure is due to the magnetic moment of the ^{55}Mn nucleus (the nuclear spin of I = 5/2).

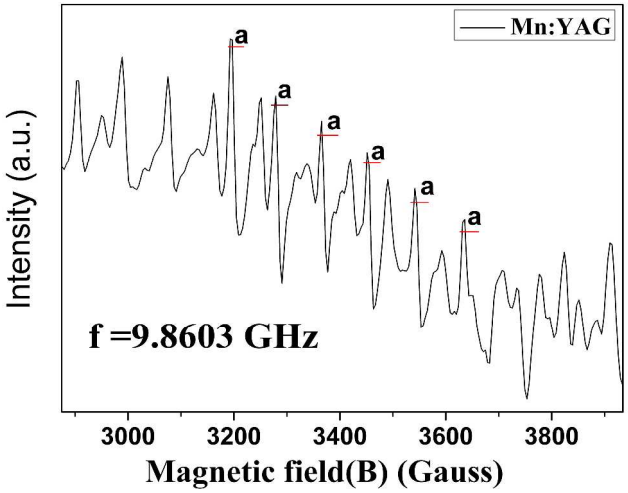

Fig.5 The hyper-fine structure of the characteristics spectra of Mn ion

In fact, as we all know, the EPR spectrum of transition metal particularly Mn is quite complex, the particular environment has considerable influence on the spin Hamiltonian parameters of the substituted ion. A number of theories have been proposed to explain the different parameters[30] and particularly the second order crystal field splittings whose origins however are not generally well understood. D. V. Azamat reported the X- and Q-band EPR measurements on $SrTiO_3$: Mn single crystals, the EPR spectrum of mixed-valence manganese(including $Mn^{2+,}$ Mn^{3+}, Mn^{4+}) was observed in the same spectrum at the same time and Mn^{4+} and Mn^{3+} can give similar EPR spectra with Mn^{2+}.[29] However, according to the characteristic hyperfine structure and resonance linewidths (about 100 G) of measured EPR spectrum of Mn: YAG and Ce, Mn: YAG crystal, we can conclude that the hyperfine structure with six lines same resonance linewidths (Fig.5) should be attributed to Mn^{2+}, however, just as what we previously refer to, actually, the multiplet structure is due to the magnetic moment of the ^{55}Mn nucleus and independent of the electronic valence of Mn, to our regret, it is a pity that the related characteristic hyperfine structure of Mn^{3+} and Mn^{4+} is not observed in our results and the possible reason is due to the used different test band frequencies and different direction of the applied magnetic field.

Absorption spectra

The absorption spectrum of as-grown and annealed in H_2 atmosphere Ce,Mn:YAG single crystal is shown in Fig.6. The wide absorption bands peaked at 458 nm and 340 nm are obviously observed in all samples and the nature of these two wide absorb bands can be attributed to 4f→5d absorption transition of Ce^{3+} in Ce,Mn:YAG single crystal.[31] Apart from the absorb band of Ce^{3+}, the absorption of Ce,Mn:YAG single crystal also consists the characteristic for Mn^{2+} and Mn^{3+}. Intensive absorption bands peaked at 279 nm can be attributed mainly to Mn^{3+}. High intensity of these absorption bands indicates that they are related to the charge transfer transitions (CTT) between O^{2-} oxygen ligands and Mn^{3+} ions (O^{2-}-Mn^{3+} CTT).[32]

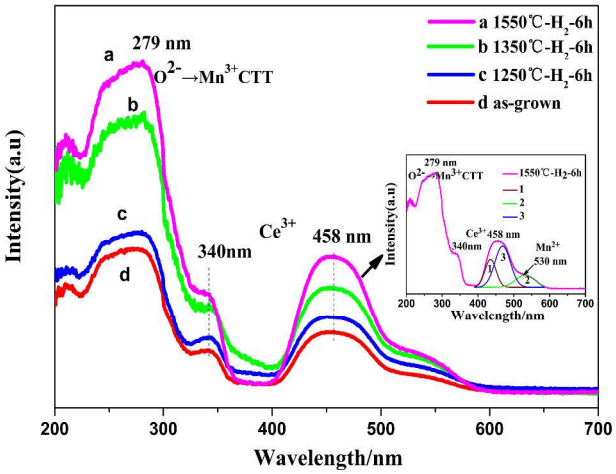

Fig.6 Absorption spectra of Mn-doped YAG:Ce single crystals annealing at different temperature

Seen from the inset in Figure 6, the absorption spectra of YAG:Ce,Mn has been decomposed into three Gaussian components with peak centers at 22988 cm^{-1} (435 nm, curve 1), 21367 cm^{-1} (468 nm, curve 3) and 18867 cm^{-1} (530 nm, curve 2), respectively. The absorption peak centers at 435 nm and 468 nm should be ascribed to the 4f→5d absorption transition of Ce^{3+},

however, the broad but weak absorption with peak centers at 18867 cm^{-1} (530 nm) should be due to $^6A_1 \rightarrow {}^4T_1$ transitions of Mn^{2+} ions.[24] To give a convincing evidence about our conclusion and clarify the absorption origin of YAG:Ce,Mn in the range of 500-600 nm, the absorption spectra of YAG:Ce and YAG:Mn (see Figure 7) are provided and compared with the YAG:Ce,Mn. The absorption spectra of YAG:Ce in range of 400-600 nm contain a broad absorption band peaking at 458 nm , which can be ascribed to the 4f→5d transition of Ce^{3+}, however, the absorption spectra of YAG:Mn in the range of 450-600 nm exhibit a broad but weak absorption band with peak centers about 525 nm, which should be due to the spin-forbidden transitions of Mn^{2+}.[23] By comparing with the absorption spectra of YAG:Ce and YAG:Mn, we can find that the absorption of YAG:Ce,Mn in the range of 500-600 nm was due to the absorption overlay of Ce^{3+} and Mn^{2+} and the weak absorption intensity of Mn^{2+} also leads to the weak absorption of YAG:Ce,Mn in range of 450-600 nm, this conclusion is also consistent with the results of Gaussian decomposition. The absorption band peaked at 458 nm related to the transitions in the lowest radiative $5d^1$ state of Ce^{3+} ions are located above the $^6A_1 \rightarrow {}^4T_1$ absorption band of Mn^{2+} ions, which can be important condition for the simultaneous energy transfer both to Mn^{2+} and Ce^{3+} ions in YAG host. Compared to the as-grown sample, it is found that the intensity of absorption band peaked at 458 nm become more intensive after annealed in H_2 atmosphere at 1250 □, 1350 □, 1550 □, respectively for 6 h. Increasing the annealing temperature, the intensity of absorption band at 458 nm become more intensive. The intensive wide absorption band covering from 440~480 nm demonstrate that as-grown YAG:Ce, Mn crystal can effectively absorb the blue light emitting by InGaN chip to be applied in the field of white LED.

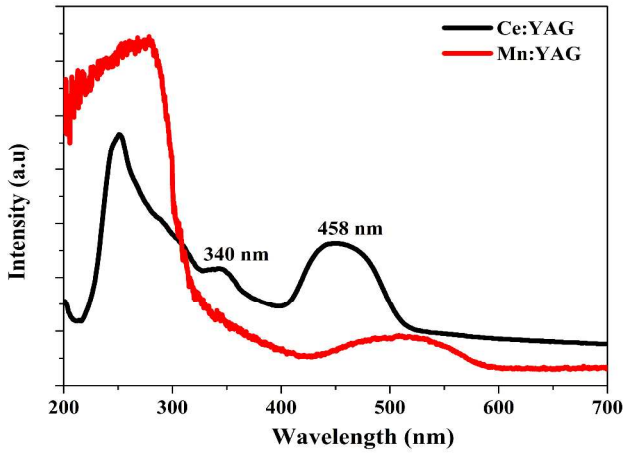

Fig.7 Absorption spectra of YAG:Ce and YAG:Mn

Photoluminescence properties

Fig.8 presents the emission spectra of Ce,Mn:YAG single crystal samples at different annealing temperatures under optical excited at 460nm. The wide emission band peaked at 530 nm is obviously observed before and after annealed in H_2, which is the characteristic peak of Ce^{3+} and can be attributed to $5d^1 \rightarrow {}^2F_{5/2}$ transition.

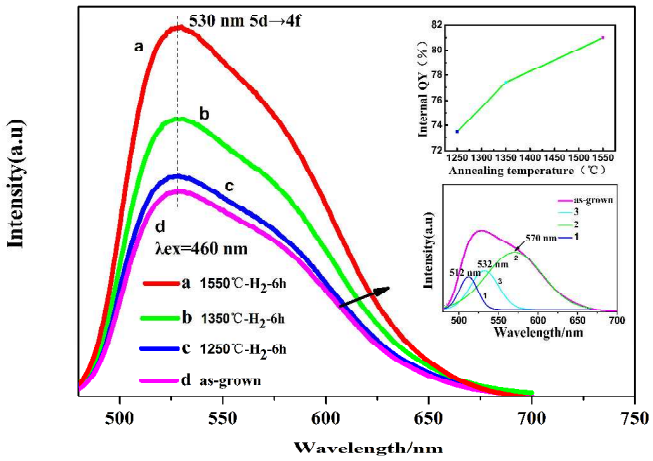

Fig.8 Emission spectra of Ce,Mn:YAG single crystal at different temperature. Inset shows the Internal quantum yield (QY) photograph of wafers under different annealing temperature.

The doublet bands of the emission spectra due to the transition of the Ce^{3+} ions from the 5d excited state to the $^2F_{5/2}$ and $^2F_{7/2}$ ground states cannot be distinguished directly. However, the emission band can be decomposed into three Gaussian components with peak centers at 19531 cm^{-1} (512 nm, curve 1), 17543 cm^{-1} (570 nm, curve 2) and 18796 cm^{-1} (532 nm, curve 3), respectively. The Gaussian profiles centered at 512 and 570 nm have an energy difference being about 1988 cm^{-1} and this energy difference is fairly well in agreement with the theoretical difference between $^2F_{5/2}$ and $^2F_{7/2}$ levels of Ce^{3+} (~2000 cm^{-1})[33]. Due to the large spatial extension of the 5d wave function, the optical spectra of Mn^{2+} in a crystal are usually broadened.[34,35,36], Furthermore, the $3d^5$ multiplet energies of Mn^{2+} in crystals depend largely on the covalency interaction with the host crystal or the crystal field. The tetrahedrally coordinated Mn^{2+} ion gives a green emission by forming a weak crystal field, while the octahedrally coordinated Mn^{2+} ion exhibits an orange-to-red emission by forming a strong crystal field[36]. To give a further analysis, the emission spectra of the prepared YAG:Ce and YAG:Mn (see Figure 9) has been added and compared with YAG:Ce,Mn.

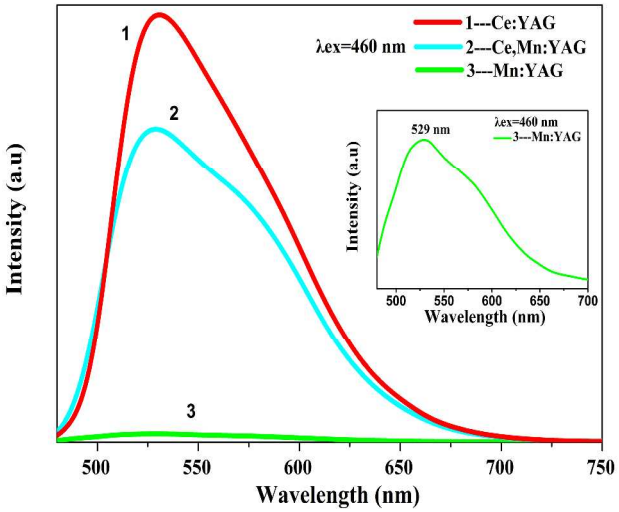

Fig.9 The emission spectra of prepared YAG:Ce,Mn,YAG:Ce and YAG:Mn

Compared with the emission spectra of YAG:Ce,Mn and YAG:Ce, upon 460 nm blue light excitation, the emission intensity of YAG:Mn is highly weak, the inset in Figure 9 shows the separated emission spectra of Mn,YAG, where a broad emission peaking at 529 nm can be observed, which demonstrate that the Gaussian components with peak centers at 532 nm in the emission spectra of YAG:Ce,Mn may be due to the $^4T_1$ (G)→$^6A_1$ (S) transition of Mn^{2+}. Due to the spin-forbidden transition effects, this green mission may be due to energy transfer from Ce^{3+} to Mn^{2+} in octahedral surrounding of Mn^{2+} ion in YAG host. Owing to YAG:Ce samples exhibits broad emission at 500–700 nm, while YAG:Mn sample shows absorption at 450–600nm. That is, there is partial overlap between Ce^{3+} emission and Mn^{2+} absorption in 500–600 nm. Therefore, it is expected that energy transfer (ET) can occur from Ce^{3+} to Mn^{2+}. Actually, much work has been done on the charge-transfer energy of Ln^{3+} in YAG[37]and the energy transfer from Ce^{3+} to different activator ions particularly Mn ion in different host lattice.[38]The relative experimental result of V. Singh et al[39]also demonstrated that Mn^{2+} activated $Y_3Al_5O_{12}$ can give green emission with peak center at 519 nm, which can be assigned to $^4T_{1g}$ (G) →$^6A_{1g}$ (S) transition of Mn^{2+} ions. In general, the luminescence spectra of Ce,Mn:YAG generally present the mixture of Ce^{3+} and Mn ions luminescence with the prevailing contribution of the Ce^{3+} emission,[39]and Mn^{2+} presents weak emission upon 460 nm blue light excitation, which make it more complex to distinguish the emission spectra of Mn^{2+}. The corresponding energy levels scheme of Ce^{3+} and Mn^{2+} ions with optical transitions and ET process are displayed in Fig.10. After Ce^{3+} firstly absorbs blue light, electron is pumped to 5d level, and then nonradiatively relaxes to the lowest component of 5d level, finally decays to $^2F_{5/2}$ and $^2F_{7/2}$ levels by radiative process, and emits green (512 nm) and yellow (570 nm) photons. Because the lowest excited 5d energy level of Ce^{3+} is

higher than the $^4T_1$ energy level of Mn^{2+}, energy transfer ET from Ce^{3+} to Mn^{2+} in YAG single crystal can easily proceed. An excited Ce^{3+} relaxes from 5d excited state to ground state nonradiatively and transfers the excitation energy to a neighboring Mn^{2+}, promoting it from $^6A_1$ ground state to $^4T_1$, after then, Mn^{2+} ion relaxes to $^6A_1$ levels nonradiatively and emits 532 nm photons corresponding to the spin-forbidden transition.[40] In our present experiment, related emission peaks of $Mn^{3+}$and Mn^{4+} are not observed under blue light excitation (λ_{ex}=460 nm), in fact, the luminescence of Mn^{2+}, Mn^{3+} and Mn^{4+} generally can be obviously observed under high-energy excitation, the 460nm blue light can not be efficiently transferred to Mn^{2+} from Ce^{3+}, which leads to the weak emission of Mn^{2+}.

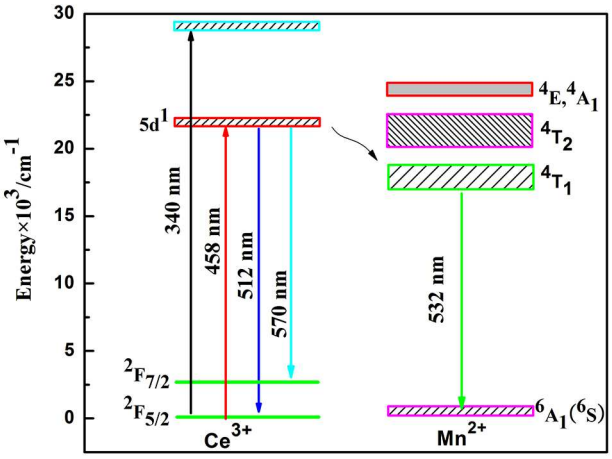

Fig.10 Illustration of the ET models for $Ce^{3+}\rightarrow Mn^{2+}$ in YAG host

Compared to the as-grown crystal sample, all emission intensity enhanced significantly. On increasing the annealing temperature, the emission intensity increase obviously and achieve the highest at 1550 □. The emission spectra demonstrate that the annealing process in H_2 atmosphere improve the luminescence properties of YAG:Ce,Mn single crystal. Inset shows the internal quantum yield (QY) of wafers under different annealing temperature. The Internal QY of as-grown sample is 72.4 %, from the diagram we can see that the Internal QY of the samples annealed in H_2 is obviously higher than that of the as-grown sample and reach the highest 81.0 % at 1550 □, which can be ascribed to more photons emitted by Ce,Mn:YAG single crystal and more intensive emission intensity, the corresponding absorption and emission spectra also confirm that.

Color-electric performance of Ce,Mn:YAG single crystal based WLEDS

The measured color-electric parameters for samples annealing in H_2 at different temperatures for 6 h, testing at 20 mA with 0.5 mm in thickness are listed in Table1.

Table 1 Color-electric performance of Ce,Mn:YAG single crystal wafers

sample	CIE	LE (lm/w)	CCT (K)	CRI	Thickness (mm)
As-grown	(0.28, 0.26)	105.25	7618	76.9	0.5
1250□	(0.29, 0.28)	110.20	5940	75.2	0.5
1350□	(0.30,0.32)	115.47	5890	74.3	0.5
1550□	(0.31,0.36)	119.93	5674	73.6	0.5

Compared to the as-grown sample, on increasing the annealing temperature, LE intensifies, CCT decreases, CRI decreases, owing to more blue light absorbed and more yellow light emitted by Ce,Mn:YAG single crystal, which is in accordance with what the absorption and emission spectra present. Obviously, increasing the annealing temperature induces monotonous intensification in the yellow luminescence, and the color coordinate of WLED shifts from white to yellow (Fig.11). For all the YAG:Ce, Mn single crystal based LED devices, the yielded luminescence is very bright, as demonstrated in the insets of Fig.9. Moreover, the LE of Mn-

doped YAG:Ce single crystal annealing at different temperature under different driven current is also tested. From the Fig.12 we can see that the measured LE changes obviously with the changed current. On increasing the driven current, the LE significantly decreases due to more blue light emitted by InGaN chip and relative less proportion of yellow light emitted by Ce,Mn:YAG single crystal.

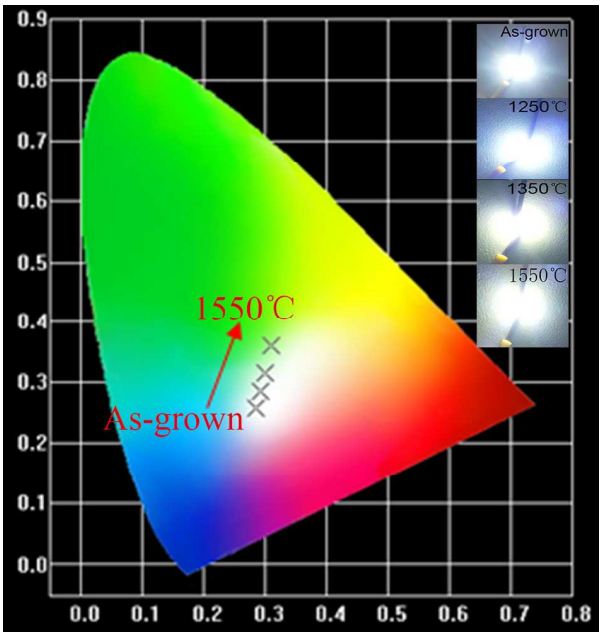

Fig.11 CIE color coordinate of the Ce,Mn:YAG single crystal wafers under different temperature, insets show luminescent photographs of the Ce,Mn:YAG single crystal wafers based WLEDs a t an operating current of 20 mA

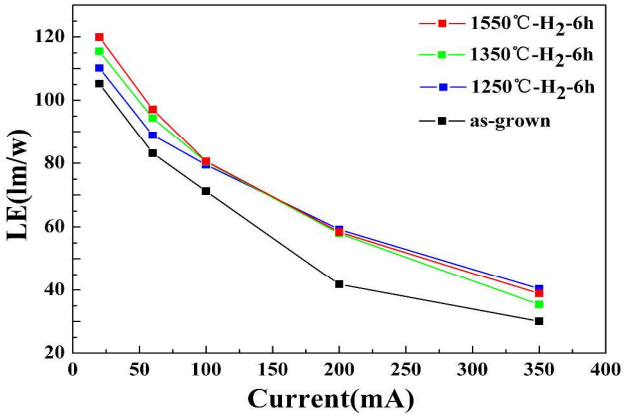

Fig.12 LE of Ce,Mn:YAG single crystal annealing at different temperature under different current

Due to the lack of a red component, the CRI of WLEDs fabricated with blue InGaN chips and YAG:Ce phosphors is low. It is reported that the CRI of pc-WLEDs could be improved by incorporating some other activators such as Mn^{2+} and Pr^{3+}. We give some illustrations of pc-WLEDs performances fabricated with Ce,Mn:YAG single crystal wafers and blue InGaN chips, as shown in Fig.13. The spectrum of the WLED is composed of blue light from the InGaN chip, 528 nm yellow light from Ce^{3+} and 564 nm orange-yellow light from Mn^{2+}. Compared to the blue LED chip and as-grown sample, on increasing the annealing temperature, the emission intensity in yellow-orange region enhance and reach the highest at 1550 □. The inset in Fig.11 illustrates this bright white light of a WLED driven at 20 mA and 3.0 V. The efficiency, color temperature, and color rendering index of the WLED are 119.93lm/W, 5674K, and 73.6, respectively. The CIE (X and Y) coordinate of the WLED is located at (x:0.31, y:0.35) which approximates to the region of white light.

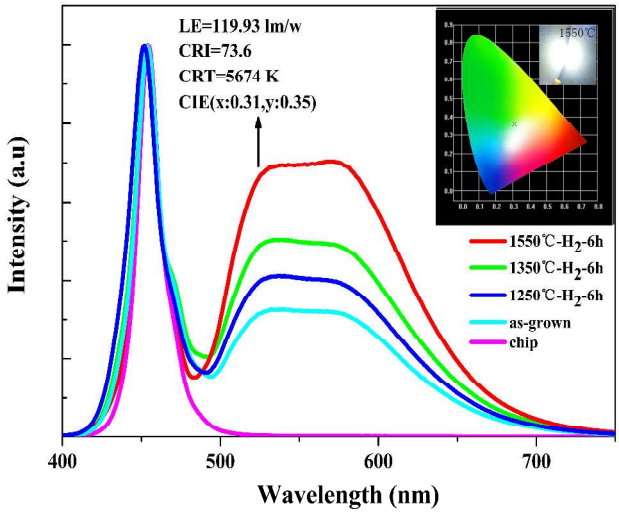

Fig.13 White luminescence spectra of the WLED fabricated with the blue InGaN chip, the annealed Ce,Mn:YAG single crystal under 1550℃ Inset: the image of a WLED at a operating current of 20 mA

Conclusions

In conclusion, the EPR spetrum of Mn ions in Czochralski grown Ce,Mn:YAG single crystal indicate that the valence state of doped manganese is mainly +2. The H_2 annealing process improves the luminescence properties of YAG:Ce,Mn single crystal for white LED. Compared to the as-grown crystal, on increasing annealing temperature, the emission intensity enhance obviously and the corresponding LE and Internal QY of the fabricated WLED intensifies, CCT decreases, CRI decreases. The H_2 annealing at 1550 ℃ is the most optimal annealing condition. After annealing, a maximum luminous efficacy reaching 119.93 lm/W, a color rendering index of 73.6 at a correlated color temperature of 5674 K is obtained, which demonstrates that Ce,Mn:YAG single crystal is expected to be an optimal candidate for white LED.

Experimental section

Ce and Mn doped YAG single crystal is grown by the Czochralski method. High purity oxide powders, Y_2O_3 (99.999%), Al_2O_3 (99.999%), CeO_2 (99.999%) and MnO_2 (99.99%), are used as starting materials. The molar ratio of Ce:Mn is 0.024:0.036. The whole growth process is in the nitrogen atmosphere. According to the chemical bonding theory of single crystal growth[41,42], the thermodynamic growth shape along [111] pulling direction is easily developed into round surface via kinetic control during large size crystal growth[41], [111] oriented YAG single crystal is thus used as a seed in this work.The pulling rate of 1.2 mm/h and the rotation rate of 15 rpm are adopted. X-ray diffraction data of sample is collected via the D8 Advance X-ray powder diffraction (Bruker) using the CuKa line (λ=0.15406 nm) 2θ ranging from 10° to 90°. The absorption spectra of polished single crystal wafer were acquired with the UV/VIS Spectrophotometer (Mode V-570, JASCO). Photoluminescence (PL) is characterized with FP-6500 fluorescence spectrometer (Japan JASCO Company). Internal QY is defined as the ratio of the emitted photons to the absorbed photons, and is measured by a spectrofluoremeter (FP-6500). An integrating sphere is mounted on the spectrofluoremeter with the entrance and exit ports located in 90° geometry, consisting of 0.5 mm Ce, Mn:YAG wafers are located in the center of the integrating sphere. The color-electric performance is characterized via the ZWL-600 light electric integrated test system. The valence of doping Mn ions is characterized by Electron Paramagnetic Resonance (A300 spectrometer, Bruker), the test frequency f =9.8603 GHz, scanning range of magnetic field B=2000~6000 G. Test samples are solid powders and the carrier tools is a capillary glass tube with a diameter of 1 mm.

Acknowledgements

The authors acknowledge financial support from National Natural Science Foundation of China (No.51172165) and National Natural Science Foundation of China (No.51372172).

References

1 G. Blasse and A. Bril, *Appl. Phys. Lett.,* 1967,**11**, 53–55.

2 X. Q. Piao, T. Horikawa, H. Hanzawa and K. Machida, *Appl. Phys. Lett.,* 2006, **88**, 161908.

3 D. Y. Wang, C. H. Huang, Y. C. Wu and T. M. Chen, *J. Mater. Chem*., 2011, **21**, 10818–10822.

4 D. L. Geng, G. G. Li, M. M. Shang, D. M. Yang, Y. Zhang, Z. Y. Cheng and J. Lin, *J. Mater. Chem.,* 2012 **22**, 14262–14271.

5 A. K, *CrystEngComm.,* 2012, **20**, 6904-6909.

6 H. S. Jang and D. Y. Jeon, *Opt. Lett.,* 2007,**32**, 3444–3446.

7 S. Ye, F. Xiao, Y. X. Pan, Y. Y. Ma and Q. Y. Zhang, *Mater. Sci. Eng. R.,* 2010, **71**, 1–34.

8 Y. C. Chiu, C. H. Huang, T. J. Lee, W. R. Liu, Y. T. Yeh, S. M. Jang and R. S. Liu, *Opt. Exp.,* 2011, **19**, 331–339.

9 N. Narendran, Y. Gu, J.P. Freyssinier, H. Yu, L. Deng, *J. Cryst. Growth.,*

2004, **268**, 449–456.

10 S. Nishiura, S. Tanabe, K. Fujioka, Y. Fujimoto, M. Nakatsuka, *Mater. Sci. Eng.,* 2009, **1,** 012031.

11 S. Nishiura, S. Tanabe, K. Fujioka, and Y. Fujimoto, *Opt. Mater.,* 2011, **33**, 688.

12 S. Nishiura and S. Tanabe, J. Ceram. Soc. Jpn., 2008, **116**, 1096.

13 N. Wei, T. C. Lu, F. Li, W. Zhang, B. Y. Ma, Z. W. Lu and J. Q. Qi, *Appl. Phys. Lett.,* 2012, **101**, 061902.

14 S. Nishiura, S. Tanabe, K. Fujioka and Y. Fujimoto, *Opt. Mater.,*2011, **33**, 688–691.

15 Batentschuk. M. Osvet, A. Schierning, G. Klier, A. Schneider, J. Winnacker, *A. Radiat. Meas.,* 2004, **38**, 539.

16 Zeng. H, Yu. Q, Wang. Z, *J. Am .Ceram. Soc.,* 2013, **96** , 2476-2480.

17 C. H. Huang and T. M. Chen, *J. PHYS. CHEM. C.,* 2011, **5**, 2349-2355.

18 Zorenko. Y, Gorbenko. V, Zorenko. T, *Opt. Mater.,* 2014, **10**, 1680-1684.

19 Singh. V, Chakradhar. R. P. S, Rao. J. L, *Appl. Phys. B.,* 2010, **2**, 407-415.

20 X. H. Zeng, G. J. Zhao, J. Xu, H. J. Li, X. M. He, H. Y. Pang, M. Y. Jie, *J. Cryst. Growth.,* 2005*,* **274,** 495–499.

21 Sun. C, Xue. D, *Scientia Sinica Technologica.,* 2014, **44**, 1674-7259.

22 Li. K, Xue. D, J. PHYS. CHEM. A., 2006, **39**, 11332-11337.

23 Zorenko. Y, Gorbenko. V, Voznyak. T, *J. Lumin.,* 2010, **130**, 380-386.

24 M. A. Noginov, G. B. Loutts, M. *J.* Warren, *Opt. Soc. Am. B.,* 1999, **16,** 475.

25 Zhao. Y. S, Zhong. J. S, Xiang. W. D, *Chinese. Sci. Bull,,* 2011, **56**, 3866-3870.

26 E. Saab, E. Abi-Aad, M. N. Bokova,, *J. Carbon.*, 2007, **45**, 561–567.

27 Q. L. Sun, X. Huang, J. P. Wu, *J. Acta. Optica. Sinica.,* 1990, **10**, 14-18.

28 Hodges. J. A, *J. Phys. Chem. Solids.,* 1974, **35**, 1385-1392.

29 Azamat. D. V, Dejneka. A, Lancok. J, *ArXiv. Preprint. ArXiv.,* 2011, **1112**, 1560.

30 Schirmer. O. F, Berlinger. W, K. A. Müller, *Solid. State. Commun*., 1975, **16**, 1289.

31 C. M. Wong, S. R. Rotman, C. Warde, *J. Appl. Phys. Lett.,* 1984, **11**, 1038–1040.

32 Zorenko. Y, Y. Z, Zorenko.Y, *Opt, Mater.,* 2014, **36**, 1680–1684.

33 C. J. Duan, Z. J. Zhang, S. Rosler, A. Delsing, J. T. Zhao and H. T. Hintzen, *Chem. Mater.,* 2011, **23**, 1851.

34 C.R. Ronda, T. Amrein, J. Lumin 69 (1996) 245.

35 L.E. Shea, R.K. Datta, J.J. Brown, J. Electrochem. Soc. 141 (1994) 1950.

36 B. Lei, Y. Liu, Z. Ye, C. Shi, J. Lumin 109 (2004) 215.

37 Li. K, Xue. D, Physica. status. solidi (b)., 2007, **6**, 1982-1987.

38 K. C. Sobha, K. J. Rao, *J. Phys. Chem. Solids.,* 1996, **57**, 1263.

39 G. Blasse, *Prog. Solid State Chem.,* 1988, **18**, 79.

40 Xie W, Tang J, Hao L, *Opt. Mater.,* 2009, **2**, 274-276.

41 Sun. C, Xue. D, *CrystEngComm.,* 2014, **11**, 2129-2135.

42 Sun. C, Xue. D, *Cryst. Growth. Des.,* 2014, **5**, 2282-2287.

Synthesis and Luminescence properties in H_2 annealing Mn-doped $Y_3Al_5O_{12}:Ce^{3+}$ single crystal for W-LEDs

Guorui Gu,[a] Weidong Xiang,*[a] Cheng Yang,[a] Xiaojuan Liang,[a]

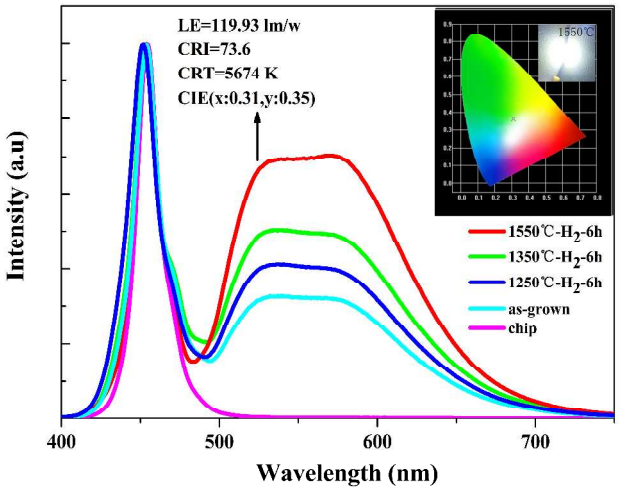

Compared to the blue LED chip and as-grown sample, on increasing the annealing temperature, the emission intensity in yellow-orange region enhance and reach the highest at 1550 □.